PHILOSOPHICAL TRANSACTIONS OF THE ROYAL SOCIETY A MATHEMATICAL, PHYSICAL & ENGINEERING SCIENCES

The S$^{\prime}$-S$^{\prime \prime}$ and H $^{\prime}$-T Minimal Surfaces and their Application to Structural Modelling of Intermediate Phases

Andrew S. Fogden

Phil. Trans. R. Soc. Lond. A 1996 **354**, 2159-2172
doi: 10.1098/rsta.1996.0096

The S′-S″ and H′-T minimal surfaces and their application to structural modelling of intermediate phases

By Andrew S. Fogden

Physical Chemistry 1, Chemical Center, PO Box 124, S-22100 Lund, Sweden

A geometric basis is presented for the analysis of possible structures of anisotropic liquid-crystalline phases of surfactant–water mixtures between the hexagonal and lamellar phase regions. As a starting point the candidates among the triply periodic minimal surfaces partitioning symmetrically distinct labyrinths are considered. The two simplest examples of this type of bicontinuous geometry are the tetragonal S′-S″ and hexagonal H′-T surfaces of genus 4. Using the exact parametrizations, their cell dimensions, vertex positions, areas and volumes are calculated. These details of the minimal surfaces are useful both in assessing the possibility of such bicontinuous intermediate phases and for generating the corresponding constant mean-curvature families which embrace other topologies, including the interesting mesh structures.

1. Introduction

Interest in surfactant–water systems is continuously renewed by the discovery of previously unknown types of aggregate phases. Transitions between hexagonal and lamellar phases have been found to involve especially intriguing structural behaviour and often pass through other lyotropic liquid-crystalline phases. Many examples of such ‘intermediates’ have been reported in the literature, although the exact geometric nature of the assemblies, and hence the actual number of distinct types, has proved difficult to establish (for a review, see Dubois-Violette & Pansu 1990).

The most familiar of the intermediates are the bicontinuous cubic phases, the structures of which are based upon a symmetric partitioning of space, sheathed by a surfactant bilayer, with water filling the pair of three-dimensional tunnel networks on either side (Hyde *et al.* 1984; Fontell 1990; Seddon & Templer 1993). It was realized that the topology of these phases could be fitted to minimal surfaces, i.e. surfaces which possess equal and opposite principal curvatures (and thus zero mean-curvature) throughout. In particular, the three space-groups commonly inferred for the cubic phases correspond to the topologically simplest schemes for bicontinuous partitioning (namely, genus 3), as represented by the three minimal surfaces P, D and G (Schwarz 1890; Schoen 1970).

A variety of anisotropic intermediates have also been observed or postulated. These include the ribbon phases (Hagslätt *et al.* 1992), which are structurally very similar to the hexagonal phase, and the mesh phases (Kekicheff & Tiddy 1989; Burgoyne *et al.* 1995; Matsen 1995), which are derivatives of the lamellar phase containing water-filled holes. In ordered mesh phases the holes are arranged in a square, hexagonal or triangular pattern (so that the hydrophobic interior of each layer forms a

Phil. Trans. R. Soc. Lond. A (1996) **354**, 2159–2172
Printed in Great Britain

two-dimensional regular network of coordination number 4, 3 or 6), and are further correlated in the normal direction. Anderson (1990) suggested that, at least in some cases, the interlayer correlation is due to the presence of a regular distribution of bridging necks. The structure would then be bicontinuous, as for the cubic phases, but now based on a non-symmetric partitioning of space into a hydrophobic network intertwined with a water-filled network. These types of bicontinuous partitions, despite remaining unbalanced by symmetry, can again be accessed with zero mean-curvature. However, the topologies of such minimal surfaces are necessarily more complicated, i.e. those with genus no lower than 4. The unbalanced minimal surfaces corresponding to the most regular distribution of mesh-bridging necks are the tetragonal S′-S″ surface and hexagonal H′-T surface of Schoen (1970), both of genus 4.

So, in the sense that P, D and G are the three simplest examples of balanced cubic minimal surfaces related to bicontinuous cubic phases, S′-S″ and H′-T are the two simplest candidates amongst the unbalanced non-cubic minimal surfaces for bicontinuous anisotropic intermediate phases. Both surfaces have been parametrized exactly by Karcher (1989), and isolated examples of the former have been constructed numerically by Anderson *et al.* (1990). In § 2 we apply the S′-S″ and H′-T parametrizations to calculation of all of the details (lengths, areas and volumes) of these surface families. This information will help in resolving the question as to whether a particular intermediate phase possesses a bicontinuous structure.

Having established a firm understanding of these minimal surfaces, the challenge is to trace their evolution as the uniform value of the mean curvature deviates from zero. This provides the complete spectrum of uniformly curved bicontinuous partitions for the given symmetry and topology. More important, as the mean curvature increases further in magnitude, these partitions undergo topological transitions. In particular, the interlayer connections neck-off to restore the corresponding mesh topologies. Thus the minimal surfaces can be used as a basis for accessing the uniformly curved manifestations of the meshes (as well as of the simpler topologies such as those of cylinders) and providing a continuous relation linking these different types of partition. These relations are illustrated in § 3.

2. The S′-S″ and H′-T minimal surfaces

Schoen (1970) hypothesized that the partition of space defined by the interpenetration of two square graphs, denoted S′ and S″, could be manifested as a minimal surface, which he called S′-S″. The basic cell generating this arrangement is the prism of mirror-planar faces illustrated in figure 1*a*; two pairs of its edges belong to the two graphs, while the intervening surface meets the other five edges at the vertices A, B, C, D and E. Schoen also proposed another minimal surface, H′-T, which is the hexagonal analogue of the tetragonal S′-S″ and is shown in figure 1*b*. The translational unit cells of the S′-S″ and H′-T surfaces, both possessing genus 4, comprise two of the layers of 8, and respectively of 12, prisms shown from above (looking down the *c*-axis) in figure 2*a*, respectively 2*b*. The space groups of these are accordingly $P4/m2/m2/m$ and $P6/m2/m2/m$, respectively.

Every minimal surface can be expressed in the parametric form

$$(x, y, z) = \mathrm{Re} \int \mathrm{d}\omega \, (1 - \omega^2, \mathrm{i}(1 + \omega^2), 2\omega) R(\omega), \tag{2.1}$$

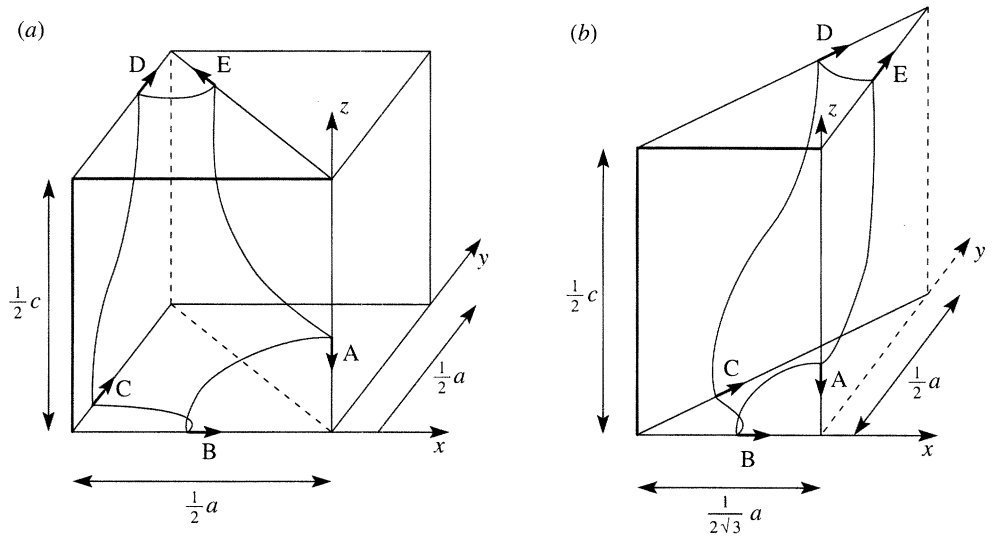

Figure 1. Illustrations of the planar-curved boundary segments of surface elements representing the (*a*) S′-S″ and (*b*) H′-T minimal surface families, showing the cell axes and dimensions, the pair of partitioned labyrinths (the first-listed in bold and the second with dashes) and the surface normal vectors at the five vertices.

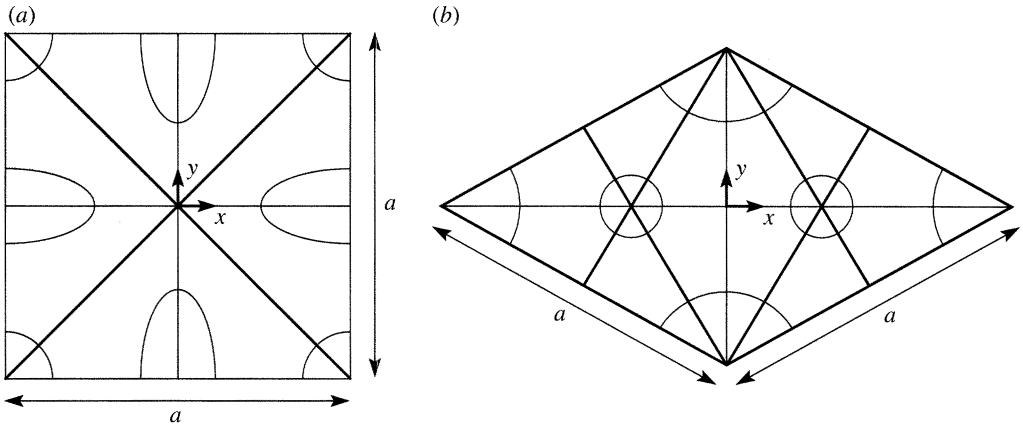

Figure 2. Plan views of the translational unit cells of the (*a*) S′-S″ and (*b*) H′-T surfaces, showing the patterns of vertical tunnels. The shadow regions correspond to the single elements in figure 1.

with some complex-analytic function $R(\omega)$ (Weierstrass 1866). Here $\omega = u + \mathrm{i}v$ is the stereographically projected Gauss map image of (x, y, z), i.e. the projection into the complex plane of the point on the unit sphere marking the unit normal $\hat{N}$ to the surface there. The S′-S″ and H′-T surfaces were proved to correspond to particular complex-analytic functions $R(\omega)$, thus verifying their existence as true minimal surfaces (Karcher 1989; Fogden & Hyde 1992*a*, *b*; Fogden 1993). We will not repeat the derivation of these functions here, but rather address the application of the results to calculation of the surface coordinates, and all properties obtained from them, via (2.1). Since the two surfaces are so similar, much of their formulation is the same. To avoid repetition we unify wherever possible in the subsequent analysis using the integer n, such that $n = 4$ (tetragonal) corresponds to S′-S″ and $n = 6$ (hexagonal) to H′-T.

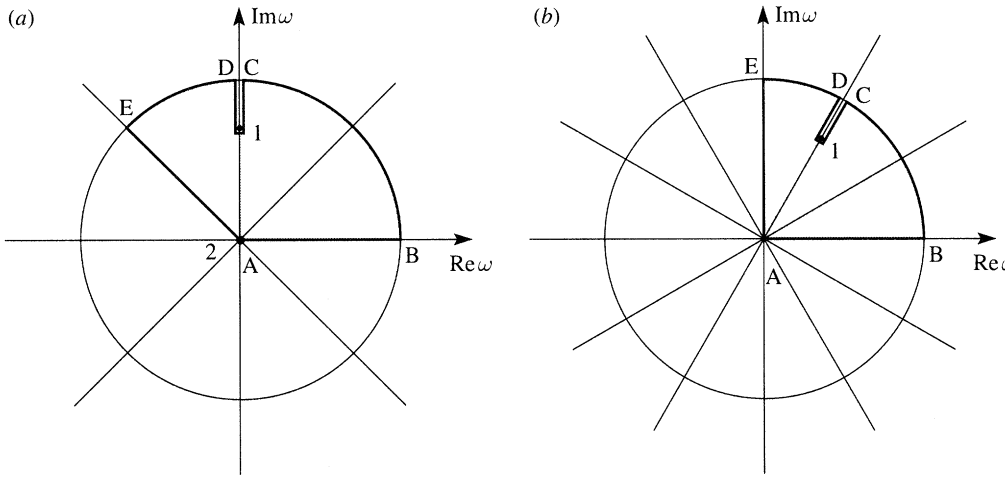

Figure 3. Geodesic triangular tilings of the unit sphere projected into the complex plane, with shading denoting the Gauss map image regions of the basic elements of the (*a*) S′-S″ and (*b*) H′-T surfaces. Letters indicate corresponding vertices in figure 1 and numerals the orders of the marked branch points.

The projected Gauss map images of the surface elements in figures 1*a* and *b*, with respect to the choice of (x, y, z) coordinate orientations there, are displayed in figures 3*a* and *b*, respectively. These images comprise three of the $(\pi/n,\ \pi/2,\ \pi/2)$ geodesic triangular tiles. In figure 1*a*, A is a flat point of order 2, and hence in figure 3*a* its image at $\omega = 0$ is the site of a second-order branch point of the $R(\omega)$ for S′-S″. On the other hand there is no such degeneracy associated with A for H′-T. Unifying, we say that a degeneracy of order $6 - n$ resides there. In addition, for both surfaces the mirror-plane curve segment CD bears a point of inflection, i.e. a flat point of order 1. The normal vector of the flat point is not fixed, but rather can swing between the directions at A and at C (or D), thus supplying the degree of freedom giving rise to the one-variable family of tetragonal or hexagonal surfaces. Thus both $R(\omega)$ possess a first-order branch point at some $\omega = \omega_0 \mathrm{e}^{\mathrm{i}2\pi/n}$, where the magnitude ω_0 can vary between zero and one, corresponding to the flat-point normal vector

$$\hat{N} = \frac{1}{(\omega_0^2 + 1)}(2\omega_0 \cos 2\pi/n, 2\omega_0 \sin 2\pi/n, \omega_0^2 - 1). \tag{2.2}$$

The face reflection of a cell in figure 1, giving the $4n$ cells comprising a translational unit (of genus 4), accordingly generates the edge reflection of the projected Gauss map image in figure 3 in such a way that the $4n$ images completely cover three copies of the complex plane. Thus the function $R(\omega)$ is triple valued for each ω, possessing a branch point of order $6 - n$ at $\omega = 0$ and $\omega = \infty$, together with first-order branch points at the $2n$ solutions of $\omega^n = \omega_0^n,\ 1/\omega_0^n$, i.e. at the roots of the polynomial

$$(\omega^n + 1)^2 - \gamma\omega^n, \quad \gamma = (\omega_0^n + 1)^2/\omega_0^n. \tag{2.3}$$

It is then found that $R(\omega)$ is given by the family of solutions of the cubic

$$\omega^{6-n}((\omega^n + 1)^2 - \gamma\omega^n)R^3 + 3\gamma^{1/3}\omega^2 R + 2 = 0. \tag{2.4}$$

The three solution branches are then given explicitly via the reduced cubic root formula

$$R = \mathrm{e}^{\mathrm{i}2m\pi/3}s_+ + \mathrm{e}^{-\mathrm{i}2m\pi/3}s_-, \quad m = 1, 2, 3, \tag{2.5}$$

where

$$s_{\pm} = \pm \frac{((\omega^n + 1) \mp ((\omega^n + 1)^2 - \gamma\omega^n)^{1/2})^{1/3}}{\omega^{(6-n)/3}((\omega^n + 1)^2 - \gamma\omega^n)^{1/2}}. \tag{2.6}$$

Substitution of (2.5) and (2.6) into (2.1) then supplies the surface coordinates (x, y, z) as explicit functions of the parameter ω for the S′-S″ or H′-T minimal surface (using $n = 4$ or $n = 6$, respectively) corresponding to a given ω_0 (and hence γ) value. Choosing each ω within the region in figure 3 generates the minimal surface piece in figure 1, from which the entire surface is obtained by reflections. This calculation must be performed for each ω_0 in the range from zero to one to give the complete families of these two surfaces. As the endpoint $\omega_0 = 0$ is reached, both surfaces degenerate to three catenoids, two of which are identical. Approaching the other extreme, $\omega_0 = 1$, the curved segment CD in figure 1 recedes without limit as it straightens vertically, and thus the surface end merges into an infinite plane. The x and y periodicities vanish and the two surfaces become 4-fold and 6-fold saddle towers.

The most important surface features—the cell dimensions, vertex positions, surface areas and enclosed volumes—of the S′-S″ and H′-T surface families are shown in figures 4*a*–7*a* and 4*b*–7*b*, respectively. In all cases the horizontal axes span the interval $0 \leqslant \omega_0 \leqslant 1$; however, we have only provided the results for the subinterval $0.06 \leqslant \omega_0 \leqslant 0.95$. As the endpoints are reached many of the curves become infinitely steep, and could only be shown fully by compressing the vertical scale and then also compressing the bridging trends of interest.

The cell dimensions a and c and the positions of the five vertices A, B, C, D and E in figure 1 are all given in a straightforward manner by evaluation of the integrals corresponding to the boundary segments AB, BC, CD, DE, EA. Since the surface is only defined up to a uniform dilation (i.e. R is only specified up to a multiplicative real constant) we consider only the ratio c/a and the vertex positions relative to their edge lengths.

The c/a ratios for the S′-S″ and H′-T families are given in figure 4. The nature of the curves are similar, rising steeply from zero at the two endpoints $\omega_0 = 0$, 1 (not shown) to reach a single maximum. The value of the maximum is 0.783 at $\omega_0 = 0.517$ for S′-S″ and 0.824 at $\omega_0 = 0.419$ for H′-T. Thus a cell ratio exceeding this cannot be achieved for a minimal surface of this type. This explains the observation of Anderson *et al.* (1990) that their numerical routine could generate S′-S″ minimal surfaces with c/a values of 0.64, 0.76 and 0.78, but not for 0.80. Any cell ratio below the maximum actually corresponds to two distinct ω_0 values, i.e. two different minimal surfaces of the given type, representing a stable/unstable pair of solutions.

We describe the vertex positions in figure 1 using the five dimensionless ordinates Z_A, X_B, Y_C, Y_D, Y_E in both cases. For S′-S″ the coordinates of the five vertices are

$$A = (0, 0, \tfrac{1}{2}cZ_A), \quad B = (-\tfrac{1}{2}aX_B, 0, 0), \quad C = (-\tfrac{1}{2}a, \tfrac{1}{2}aY_C, 0),$$

$$D = (-\tfrac{1}{2}a, \tfrac{1}{2}aY_D, \tfrac{1}{2}c), \quad E = (-\tfrac{1}{2}aY_E, \tfrac{1}{2}aY_E, \tfrac{1}{2}c),$$

while for H′-T we have

$$A = (0, 0, \tfrac{1}{2}cZ_A), \quad B = \left(-\frac{a}{2\sqrt{3}}X_B, 0, 0\right), \quad C = \left(-\frac{a}{2\sqrt{3}}(1 - Y_C), \tfrac{1}{2}aY_C, 0\right),$$

$$D = \left(-\frac{a}{2\sqrt{3}}(1 - Y_D), \tfrac{1}{2}aY_D, \tfrac{1}{2}c\right), \quad E = (0, \tfrac{1}{2}aY_E, \tfrac{1}{2}c).$$

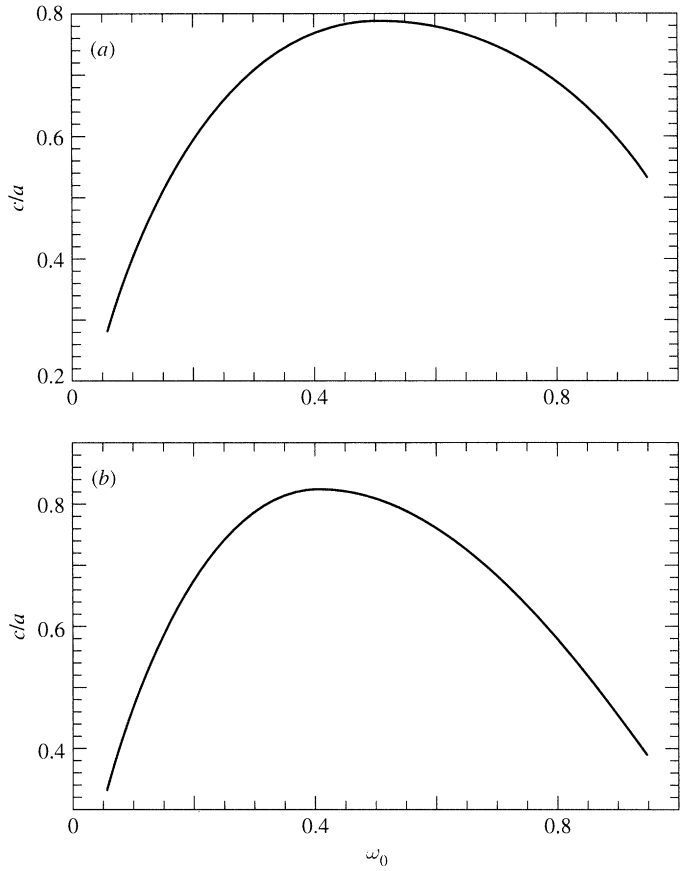

Figure 4. Ratios of the vertical to the horizontal translation lengths for the (*a*) S′-S″ and (*b*) H′-T minimal surface families.

For both S′-S″ and H′-T it can be shown analytically that $Z_{\mathrm{A}} = \frac{1}{3}$ for all family members $0 \leqslant \omega_0 \leqslant 1$, so that the point A is fixed throughout at $\frac{1}{3}$ of the way up its cell edge in figure 1. The other four vertices slide along their edges with varying ω_0 as shown in figure 5. As ω_0 approaches zero the variable Y_{C} decreases to zero while X_{B}, Y_{D}, Y_{E} all increase to one. At the other extreme all four variables decrease to zero as ω_0 tends to one.

The surface areas $\mathrm{S_p}$ of the minimal surface pieces in figure 1 are given by the formula

$$\mathrm{S_p} = \iint_{\Omega} \mathrm{d}u\,\mathrm{d}v\,(1+|\omega|^2)^2|R(\omega)|^2, \tag{2.7}$$

in which Ω denotes the corresponding region of the (u, v) parameter space, namely the image regions in figure 3 comprising the three $(\pi/n,\ \pi/2,\ \pi/2)$ triangles. To simplify the integral it serves to apply a reflection or rotation, mapping two of the triangles into the other, so that the integration range becomes the single triangle Δ. For example, the reflection $\mathrm{e}^{\mathrm{i}2\pi/n}\bar{\omega}$ of the second triangle and the rotation $\mathrm{e}^{-\mathrm{i}2\pi/n}\omega$ of the third carries both into the first triangle. Then the integration of the appropriate branch of $|R(\omega)|^2$ over Ω in (2.7) is equivalent to integrating the sum of all three

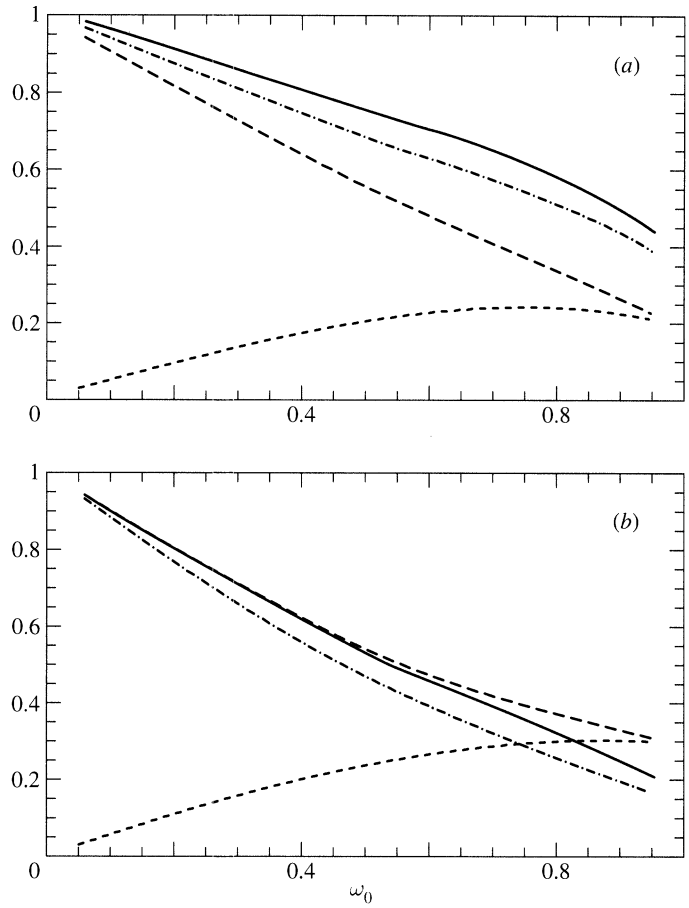

Figure 5. Ordinates specifying the positions of the vertices B, C, D and E, relative to their cell edge lengths, for the (*a*) S′-S″ and (*b*) H′-T minimal surface families: ——, X_B; - - - -, Y_C; – – –, Y_D; – · – · –, Y_E.

branches of it over Δ:

$$S_p = \iint_{\Delta} du\, dv\, (1+|\omega|^2)^2 \sum_{m=1}^{3} |R(\omega)|^2. \tag{2.8}$$

Substitution of (2.5) then gives, on switching to polar coordinates $\omega = re^{i\theta}$,

$$S_p = 3\int_0^{\pi/n} d\theta \int_0^1 dr\, r(1+r^2)^2(|s_+(\omega)|^2 + |s_-(\omega)|^2). \tag{2.9}$$

Inserting the $s_\pm$ from (2.6) then gives the surface area of the single piece (in figure 1) of S′-S″ (for $n=4$) and H′-T (for $n=6$).

From these surface areas, together with the cell lengths a and c already determined, we calculate the dimensionless surface–volume ratios $\sigma = S/V^{2/3}$. We multiply the ratios for the single pieces by $(4n)^{1/3}$ to give the values for the full translational units possessing genus 4. Thus for S′-S″ we have

$$\sigma = \frac{16S_p}{(a^2c)^{2/3}}, \tag{2.10}$$

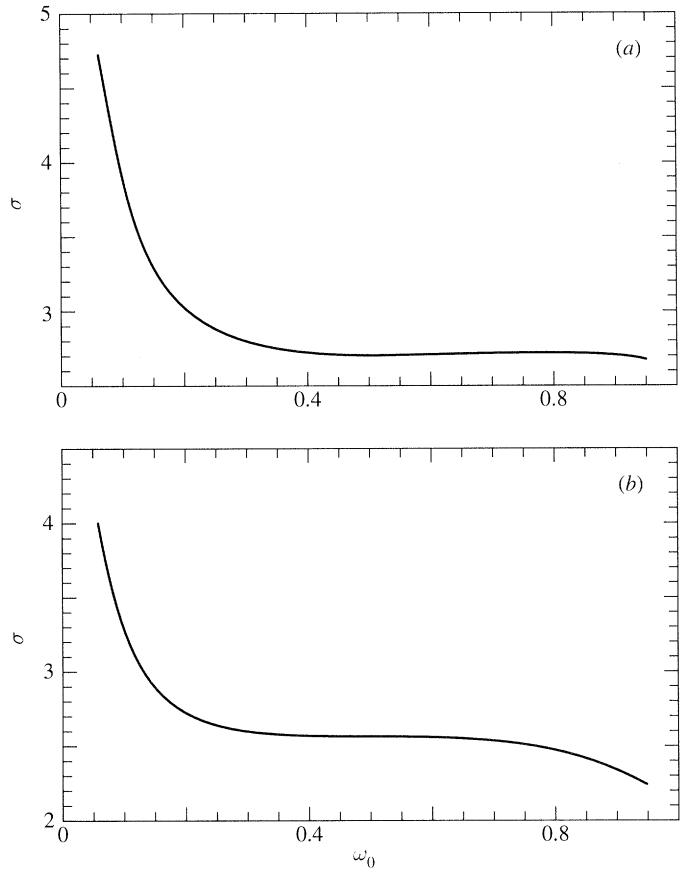

Figure 6. Dimensionless surface/volume ratios for the translational unit cells of the (*a*) S′-S″ and (*b*) H′-T minimal surface families.

while for H′-T

$$\sigma = \frac{24\mathrm{S_p}}{(\sqrt{3}a^2c/2)^{2/3}}. \tag{2.11}$$

The results given in figure 6 are again quite similar for the two families. In both cases σ diverges to infinity as $\omega_0 = 0$ is approached, and drops sharply to zero as ω_0 tends to one. These two extremes are connected by a very flat middle section which displays a shallow minimum followed by a shallow maximum. For S′-S″ the local minimum is 2.708 at $\omega_0 = 0.520$ and the local maximum is 2.723 at $\omega_0 = 0.758$. For H′-T the local minimum is 2.574 at 0.422 and the local maximum is 2.576 at 0.493. The S′-S″ surfaces numerically generated by Anderson *et al.* (1990) for the isolated c/a values of 0.64 and 0.76 give equal σ values of 2.718. This is in agreement with our results in figure 6*a*, provided that these c/a values are taken to correspond to the surfaces given by the ω_0 values to the right of the maximum in figure 4*a*. The simple approximation $\sigma = (9\pi(g-1)/4)^{1/3}$ of Hyde (1990) for periodic minimal surfaces, derived by assuming perfect homogeneity in the Gaussian curvature, gives 2.768 for genus 4 surfaces. This number is quite close to the values over the middle sections in figure 6, more so for the S′-S″ than the H′-T surfaces.

Determination of the volumes partitioned by a minimal surface is more involved

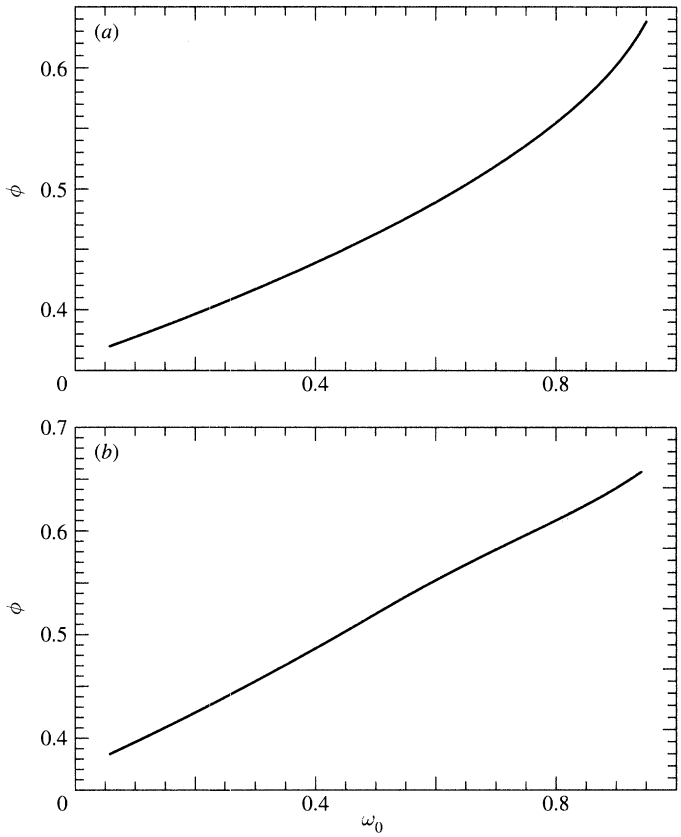

Figure 7. Fractions of the translational unit cell volumes of the (*a*) S′-S″ and (*b*) H′-T minimal surface families occupied by the second-listed labyrinth.

since it entails integration through space. For the pieces in figure 1 we calculate the subvolume V_p of the cell corresponding to the S″ labyrinth in (*a*) and the T labyrinth in (*b*). In both cases it is convenient to sweep-out space in the z-direction and split the subvolume into two such parts:

$$V_\mathrm{p} = V_1 + V_2. \tag{2.12}$$

Here V_1 is the volume of the vertical tube wedge, given by the area of the top face enclosed by the segment DE multiplied by the cell height $\frac{1}{2}c$. In this way V_1 can be expressed as

$$V_1 = \tfrac{1}{2}c\int_0^{\pi/n} \mathrm{d}\theta\, f(\theta)\Big\{2^{-(6-n)/4}\cos\theta\int_0^{\pi/n}\mathrm{d}\theta'\cos(\theta'-(\pi/n))f(\theta') + \tfrac{1}{2}\int_0^{\theta}\mathrm{d}\theta'\sin(\theta-\theta')f(\theta')\Big\}, \tag{2.13}$$

in which f is the real-valued function

$$f(\theta) = \frac{4\gamma^{1/6}}{(\gamma - 4\cos^2 n\theta/2)^{1/2}}\sin\frac{1}{3}\left\{\pi + ar\cos\left(\frac{2\cos n\theta/2}{\gamma^{1/2}}\right)\right\}. \tag{2.14}$$

The second contribution V_2 is then the volume traced by projection of the surface

piece onto the bottom face of the cell. This is given by

$$V_2 = \iint_{\Omega} \mathrm{d}u\,\mathrm{d}v\,(1-|\omega|^4)|R(\omega)|^2\left\{\tfrac{1}{2}cZ_\mathrm{A} + \mathrm{Re}\int_0^\omega \mathrm{d}\omega'\,2\omega' R(\omega')\right\}. \tag{2.15}$$

The mapping of Ω to Δ used to transform (2.7) to (2.8) produces a similar simplification here:

$$V_2 = \iint_{\Delta} \mathrm{d}u\,\mathrm{d}v\,(1-|\omega|^4)\sum_{m=1}^{3}\left(|R(\omega)|^2\left\{\tfrac{1}{2}cZ_\mathrm{A} + \mathrm{Re}\int_0^\omega \mathrm{d}\omega'\,2\omega' R(\omega')\right\}\right). \tag{2.16}$$

Again, inserting (2.5) and adopting polar coordinates we finally obtain

$$V_2 = 3\int_0^{\pi/n}\mathrm{d}\theta\int_0^1 \mathrm{d}r\,r(1-r^4)\left\{\tfrac{1}{2}cZ_\mathrm{A}(|s_+(\omega)|^2+|s_-(\omega)|^2)\right.$$
$$\left. + \mathrm{Re}\left(\mathrm{e}^{\mathrm{i}2\theta}\int_0^r \mathrm{d}r'\,2r'(s_+(\omega)\bar{s}_-(\omega)s_+(\omega') + s_-(\omega)\bar{s}_+(\omega)s_-(\omega'))\right)\right\}. \tag{2.17}$$

Evaluating V_1, V_2 and hence V_p, the volume partitioning $1-\phi$, ϕ for the two labyrinths of the S′-S″ surface ($n=4$) is then given by

$$\phi = 16V_\mathrm{p}/(a^2c), \tag{2.18}$$

and that for the H′-T surface ($n=6$) by

$$\phi = 16\sqrt{3}V_\mathrm{p}/(a^2c). \tag{2.19}$$

The results for the two families of surfaces are given in figure 7. In the extremes, which are again not shown, ϕ turns sharply down to zero as ω_0 approaches zero, and up to one as ω_0 tends to one. In the middle sections ϕ rises steadily with ω_0. The crossover point, $\phi=0.5$, at which the sides switch from minority to majority shares, occurs at $\omega_0=0.65$ for S′-S″ and at $\omega_0=0.45$ for H′-T; the values $\phi(\omega_0)$ for S′-S″ are in fact very close to $\phi(\omega_0-0.2)$ for H′-T over a significant part of this range.

3. Applications and extensions

The foregoing presentation of all quantitative details for the minimal surfaces of S′-S″ and H′-T types is useful for a number of reasons. The surfaces only contain a single degree of freedom (ω_0) with which all of the known compositional and structural specifics of a particular intermediate phase can be fitted. Thus an assessment of whether or not the phase matches an S′-S″ or H′-T family member is straightforward. The known volume fraction of the partitioned components immediately dictates that only two values of ω_0 are possible—those corresponding to either ϕ or $1-\phi$ (depending on the assignment of labyrinths) in figure 7. Any such ω_0 possesses a unique value of σ in figure 6, of c/a in figure 4, and of the scaled positions for the four variable vertices in figure 5. If the actual dimensions a and c are known, from indexation of the scattering data with these space-groups (numbers 123 and 191), then comparison with the above quantities immediately reveals whether the predictions are consistent and, moreover, allow physically reasonable packing dimensions.

As mentioned in the introduction, the main purpose of deriving the minimal surfaces is to extend this knowledge of the zero mean-curvature (H = 0) case to construction of the related surfaces possessing non-zero constant values of H throughout.

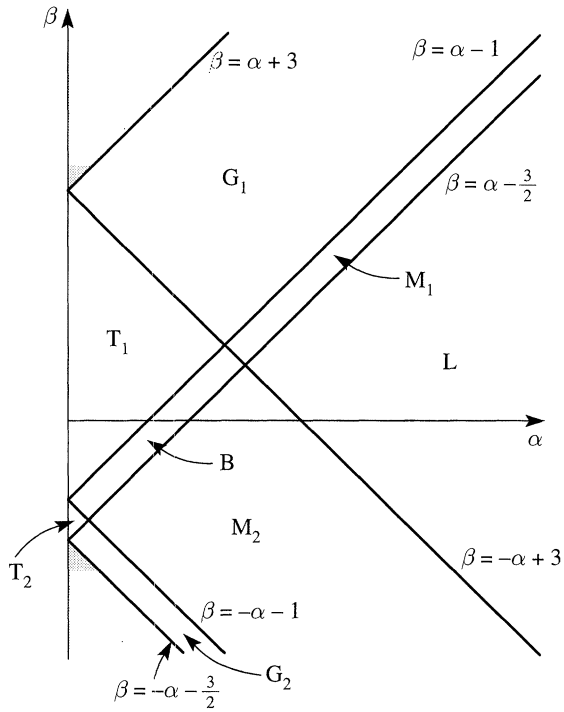

Figure 8. Topology diagram for the level surfaces $t_1 + \alpha t_2 = \beta$ given by the two simplest trigonometric terms (3.3) for P6/m2/m2/m symmetry, showing the eight regions of the (α, β) half-plane corresponding to distinct topology types; no surfaces exist for the upper and lower shaded regions.

This extension poses mathematical problems since the property of conformality (angle preservation) of the Gauss map, common to all minimal surfaces, is not shared by the surfaces with $H \neq 0$. Thus, although an analogue of the Weierstrass representation (2.1) has been proved to exist for this broader class, the functions involved are no longer purely complex-analytic and are accordingly much more difficult to determine (Gackstatter 1990). One alternative is to proceed numerically using the general computational method developed by Anderson *et al.* (1990). This method has been successful in deriving the entire set of constant H relatives of various cubic minimal surfaces, together with isolated relatives of S′-S″ surfaces.

Another approach is to abandon the parametric description and instead define the surface implicitly by

$$f(X, Y, Z) = 0, \tag{3.1}$$

with the function f written as a Fourier series for the particular space-group of the constant H surface set. To illustrate the procedure we consider the space-group 191 ($P6/m2/m2/m$) of H′-T and its relatives (identical considerations can be applied to S′-S″). The lowest frequency terms in the series

$$f(X, Y, Z) = a_0 + a_1 t_1 + a_2 t_2 + \cdots \tag{3.2}$$

are then given by

$$t_1 = \cos \mu X + \cos \mu(\tfrac{1}{2}X + \tfrac{1}{2}\sqrt{3}Y) + \cos \mu(\tfrac{1}{2}X - \tfrac{1}{2}\sqrt{3}Y), \quad t_2 = \cos \lambda Z. \tag{3.3}$$

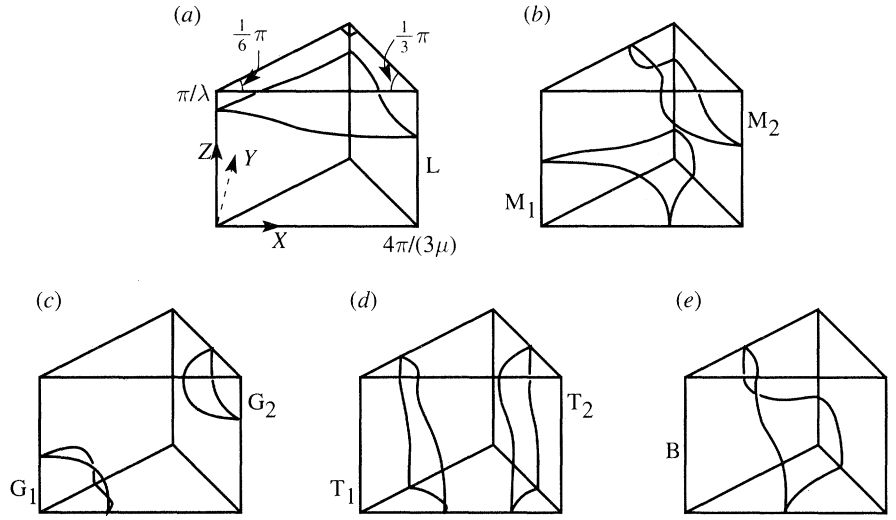

Figure 9. The basic unit cell with respect to the (X, Y, Z) coordinates, together with representative surfaces given by α, β values within each of the eight topology regions (*a*) L, (*b*) M_1, M_2, (*c*) G_1, G_2, (*d*) T_1, T_2 and (*e*) B, in figure 8.

Here $\mu = 4\pi/(\sqrt{3}a)$ and $\lambda = 2\pi/c$ and we have transformed coordinates from (x, y, z) in figure 1*b* to (X, Y, Z) for convenience.

It is useful to initially consider the surfaces obtained by taking only these first three terms in the series. These surfaces then possess three degrees of freedom aside from uniform dilation, given by $\alpha = a_2/a_1$, $\beta = -a_0/a_1$ and the stretching ratio μ/λ. As α and β are varied the surfaces smoothly pass through topological transitions, thus spanning many types of topology. These different types can be simply determined by considering the nature of the surface intersection with the edges of the basic cell. This analysis gives the diagram in figure 8, indicating the eight subregions of (α, β) space corresponding to different topological types, labelled B, T_1, T_2, G_1, G_2, M_1, M_2, L. Figures 9*a*–*e* display representative surface pieces of each of these types.

Note that all eight topology types can be achieved with constant H. Type B corresponds to the H′-T minimal surface and its non-zero H variants. Types T_1, T_2 and G_1, G_2 correspond to packings of cylinders, or more generally of Delaunay unduloids of revolution, and of spheres, respectively. The triangular and hexagonal meshes, M_1 and M_2, have been proven by Lawson (1970) to be attainable with constant H, although their exact surface equations remain unknown. Finally, type L is represented by the plane. This truncation of the Fourier series thus demonstrates the possible evolution of the H′-T minimal surface through these topological transformations as H is increased or decreased from zero. In terms of the implicit surface definition in (3.1) the condition for constant H is

$$2H = G/((f_X^2 + f_Y^2 + f_Z^2)^{3/2}), \tag{3.4}$$

in which the numerator is

$$G = (f_Y^2 + f_Z^2)f_{XX} - f_X(f_Y f_{XY} + f_Z f_{XZ}) + (f_Z^2 + f_X^2)f_{YY} - f_Y(f_X f_{XY} + f_Z f_{YZ}) + (f_X^2 + f_Y^2)f_{ZZ} - f_Z(f_X f_{XZ} + f_Y f_{ZY}). \tag{3.5}$$

Clearly any Fourier series containing only a finite number of terms cannot be a (non-trivial) exact solution of (3.4), (3.5). A previous study (Fogden & Lidin 1994)

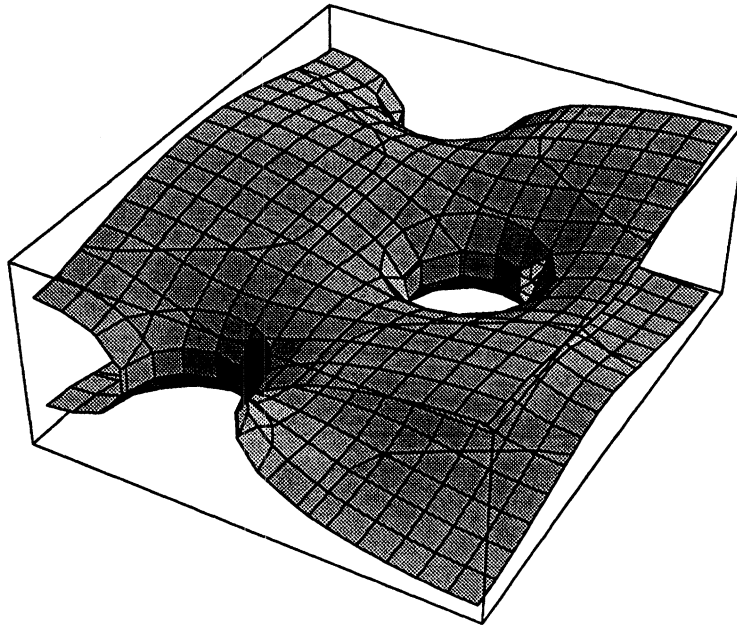

Figure 10. Piece of the triangular (6-connected) mesh surface with constant mean curvature value $\mathrm{H} = -0.9/a$.

showed that truncated Fourier series can give good approximations to minimal surfaces. In particular, for the space-group $Im\bar{3}m$ it was found that the corresponding three-term truncation could be matched, using only the one variable, with great accuracy to the P surface. However, the H′-T surface and its constant mean-curvature companions differ from the P minimal surface in that they are unbalanced and bounded only by mirror-planar curves, as opposed to two-fold straight lines (which then guarantee exact boundary matching by symmetry). So in the present case a great many more terms will need to be included to achieve such accuracy.

It is possible though to use the exact parametrization of the H′-T minimal surface family in § 2 to obtain any number of its Fourier terms. This can then be used as a starting point for determining the contant mean curvature companions by iterating (3.4), (3.5) and tracking the solution as H is incremented, using a numerical method similar to that of Mackay (1994). Using such an approach, accurate approximations to the hexagonal and triangular mesh surfaces contained in the constant H set of the H′-T surface family have been obtained (Fogden & Stenkula 1996). As an example, figure 10 displays the member of the triangular mesh surfaces (i.e. type M_1 in figures 8 and 9) corresponding to the constant value $\mathrm{H} = -0.9/a$ (where a is the horizontal translational length), generated using 24 terms in the Fourier series.

References

Anderson, D. M. 1990 A new technique for studying microstructures. *J. Physique Colloq.* C **51**, 1–18.

Anderson, D. M., Davis, H. T., Scriven, L. E. & Nitsche, J. C. C. 1990 Periodic surfaces of prescribed mean curvature. *Adv. Chem. Phys.* **77**, 337–396.

Burgoyne, J., Holmes, M. C. & Tiddy, G. J. T. 1995 An extensive mesh phase liquid crystal in aqueous mixtures of a long chain nonionic surfactant. *J. Phys. Chem.* **99**, 6054–6063.

Dubois-Violette, E. & Pansu, B. (eds) 1990 International Workshop on Geometry and Interfaces. *J. Physique Colloq.* C **51**.

Fogden, A. S. 1993 Parametrisation of triply periodic minimal surfaces. III. General algorithm and specific examples for the irregular class. *Acta Crystallogr.* A **49**, 409–421.

Fogden, A. S. & Hyde, S. T. 1992*a* Parametrisation of triply periodic minimal surfaces. I. Mathematical basis of the construction algorithm for the regular class. *Acta Crystallogr.* A **48**, 442–451.

Fogden, A. S. & Hyde, S. T. 1992*b* Parametrisation of triply periodic minimal surfaces. II. Regular class solutions. *Acta Crystallogr.* A **48**, 575–591.

Fogden, A. S. & Lidin, S. 1994 Description of cubic liquid-crystalline structures using simple surface foliations. *J. Chem. Soc. Faraday Trans.* **90**, 3423–3431.

Fogden, A. S. & Stenkula, M. 1996 (In preparation.)

Fontell, K. 1990 Cubic phases in surfactant and surfactant-like lipids. *Colloid Polym. Sci.* **268**, 264–285.

Gackstatter, F. 1990 H. Hopf's quadratic differential and a Weierstrass formula for general surfaces and surfaces of constant mean curvature. *J. Physique Colloq.* C **51**, 163–168.

Hagslätt, H., Söderman, O. & Jönsson, B. 1992 The strucure of intermediate ribbon phases in surfactant systems. *Liquid Cryst.* **12**, 667–688.

Hyde, S. T. 1990 Curvature and the global structure of interfaces in surfactant-water systems. *J. Physique Colloq.* C **51**, 209–228.

Hyde, S. T., Andersson, S., Ericsson, B. & Larsson, K. 1984 A cubic structure consisting of a lipid bilayer forming an infinite periodic minimal surface of the gyroid type in the glycerolmonooleate-water system. *Z. Kristallogr.* **168**, 213–219.

Karcher, H. 1989 The triply-periodic minimal surfaces of Alan Schoen and their constant mean curvature companions. *Manuscr. Math.* **64**, 291–337.

Kekicheff, P. & Tiddy, G. J. T. 1989 Structure of the intermediate phase and its transformation to lamellar phase in the lithium perfluorooctanoate/water system. *J. Phys. Chem.* **93**, 2520–2526.

Lawson, H. B. 1970 Complete minimal sufaces in S3. *Ann. Math.* **92**, 335–374.

Mackay, A. L. 1994 Periodic minimal surfaces from finite element methods. *Chem. Phys. Lett.* **221**, 317–321.

Matsen, M. W. 1995 Stabilising new morphologies by blending homopolymer with block copolymer. *Phys. Rev. Lett.* **74**, 4225–4228.

Schoen, A. H. 1970 Infinite periodic minimal surfaces without self-intersections. NASA techical note, TD-5541.

Schwarz, H. A. 1890 *Gesammelte Mathematische Abhandlungen.* Berlin: Springer.

Seddon, J. M. & Templer, R. H. 1993 Cubic phases of self-assembled aggregates. *Phil. Trans. R. Soc. Lond.* A **344**, 377–401.

Weierstrass, K. 1866 Untersuchungen über die Flächen, deren mittlere Krümmung überall gleich Null ist. *Monatsber. Berliner Akad.*, pp. 612–625.

PHILOSOPHICAL TRANSACTIONS OF THE ROYAL SOCIETY A MATHEMATICAL, PHYSICAL & ENGINEERING SCIENCES